

COMPARING THE OBSERVABLE PROPERTIES OF DWARF GALAXIES ON AND OFF THE ANDROMEDA PLANE

MICHELLE L. M. COLLINS^{1,2,3}, NICOLAS F. MARTIN^{4,1}, R. M. RICH⁵, RODRIGO A. IBATA⁴, SCOTT C. CHAPMAN⁶, ALAN W. MCCONNACHIE⁷, ANNETTE M. FERGUSON⁸, MICHAEL J. IRWIN⁹, GERAINT F. LEWIS¹⁰

Draft version June 3, 2022

ABSTRACT

The thin, extended planes of satellite galaxies detected around both the Milky Way and Andromeda are not a natural prediction of the Λ CDM paradigm. Galaxies in these distinct planes may have formed and evolved in a different way (e.g., tidally) to their off-plane neighbours. If this were the case, one would expect the on- and off-plane dwarf galaxies in Andromeda to have experienced different evolutionary histories, which should be reflected by the chemistries, dynamics, and star formation histories of the two populations. In this work, we present new, robust kinematic observations for 2 on-plane M31 dSphs (And XVI and XVII) and compile and compare all available observational metrics for the on- and off-plane dwarfs to search for a signal that would corroborate such a hypothesis. We find that, barring their spatial alignment, the on- and off-plane Andromeda dwarf galaxies are indistinguishable from one another, arguing against vastly different formative and evolutionary histories for these two populations.

Subject headings: dark matter — galaxies: dwarf — galaxies: fundamental parameters — galaxies: kinematics and dynamics — Local Group

1. INTRODUCTION

Dwarf spheroidal galaxies (dSphs) offer an insight into how the faintest galaxies in the Universe have evolved over the course of cosmic time. Those bright enough to permit the detailed study of their resolved stellar populations are relatively nearby (distances from $\sim 20 - 1000$ kpc), and allow us to learn much about both their luminous structure and their dark matter halos.

Such studies have shown that these galaxies follow trends observed in more massive systems. Work by e.g., Tolstoy et al. (2009) and Brasseur et al. (2011) demonstrated that Local Group (LG) dSphs follow a well-defined size-luminosity relationship that matches onto that of more massive late-type galaxies. They also obey a mass-metallicity relation (Kirby et al. 2011, 2013b) that ties on smoothly to that followed by dwarf irregular galaxies. Additionally, dSphs follow a well-defined size-velocity dispersion relation (Collins et al. 2014) that appears to be an extrapolation of the mean rotation curve of spiral galaxies, indicative of a mass-radius relation that holds over many orders of magnitude in mass (Walker

et al. 2010).

Such relations might encourage us to think that these systems are simple to understand. But a number of unexpected results have been unearthed in these studies also. One particularly surprising result is the spatial alignment of dwarf galaxies around the Milky Way (MW) and Andromeda (M31). The majority of known MW dSphs appear to delineate a vast (diameter ~ 300 kpc), thin (rms scale height ~ 40 kpc) plane structure, with a polar orientation with respect to the MW disk (e.g., Lynden-Bell 1976; Pawlowski et al. 2012, 2013). Similarly, studies of M31 using data from the Pan-Andromeda Archaeological Survey (PAndAS) have revealed that $\sim 40\%$ of its dwarf galaxies are aligned in a vast (diameter ~ 400 kpc), thin (rms scale height ~ 14 kpc), rotating plane (Ibata et al. 2013; Conn et al. 2013). Since this work, 3 more M31 dSphs have been discovered using PanSTARRS (Martin et al. 2013b,a), one of which (Cas III) also appears to lie in the plane, but is counter-rotating (Martin et al. 2014). Such highly ordered substructure is not a strong prediction from cosmological simulations, where the probability of finding such thin, extended planes is $\sim 10^{-4}$ (Ibata et al. 2014b; Pawlowski et al. 2014, Millennium II simulations). Also, recent work suggests that planes, or ordered motion of satellites, may be extremely common in both the Local Universe, and out to $z \sim 0.2$ (Pawlowski et al. 2013; Bellazzini et al. 2013; Ibata et al. 2014a). As a result, concern has been raised as to whether the Λ -cold dark matter (Λ CDM) paradigm can reproduce the structured nature of substructure. In response, alternative scenarios have been put forth to explain these planar structures, without resting on a CDM foundation.

One such mechanism arose from Hammer et al. (2010), where the morphology of the M31 system is explained as the result of an ancient, gas-rich merger. Follow up work by Hammer et al. (2013) demonstrated that this simulation naturally reproduces a disk of tidally created dwarf galaxies along the orbit of the merger, morphologically

¹ Max-Planck-Institut für Astronomie, Königstuhl 17, D-69117 Heidelberg, Germany

² Astronomy Department, Yale University, New Haven, CT 06510, USA

³ Hubble Fellow

⁴ Observatoire de Strasbourg, 11, rue de l'Université, F-67000, Strasbourg, France

⁵ Department of Physics and Astronomy, University of California, Los Angeles, CA 90095-1547

⁶ Dalhousie University Dept. of Physics and Atmospheric Science, Coburg Road Halifax, B3H1A6, Canada

⁷ NRC Herzberg Institute of Astrophysics, 5071 West Saanich Road, British Columbia, Victoria V9E 2E7, Canada

⁸ Institute for Astronomy, University of Edinburgh, Royal Observatory, Blackford Hill, Edinburgh, EH9 3HJ, UK

⁹ Institute of Astronomy, Madingley Rise, Cambridge, CB3 0HA, UK

¹⁰ Sydney Institute for Astronomy, School of Physics, A28, University of Sydney, NSW 2006, Australia

similar to that observed by Ibata et al. (2013). These dwarf galaxies were created during the merger (5–8 Gyr ago) in the gas rich tidal tails. As a result, they would not be dark matter dominated, and would have formed in a very different manner to dwarf galaxies off the plane, which should have formed within their own dark matter halos.

Such a scenario should be testable purely by comparing the properties of dwarf galaxies both on and off the plane. Notwithstanding the question of survivability of such tidal dwarf galaxies for Gyrs, the vastly different formative histories should lead to differences in the kinematic, chemical and star-forming properties of the 2 different populations. Such a comparison is only possible in M31 as, so far, the vast majority of the identified MW dSphs have been associated with the plane of satellites, leaving few (cf. Sagittarius) off-plane objects for comparison.

In this *Letter*, we compare observational properties (sizes, luminosities, masses, metallicities and star formation histories) of dSphs in the M31 system. In order for the comparison to be robust, we fold in new kinematic data for 2 on-plane dSphs, And XVI and XVII, allowing more secure derivations of their properties. In §2 we present our observations and analysis of And XVI and XVII; in §3, we compare the properties of dSphs on- and off- the Andromeda plane of satellites and we summarise our findings in §4.

2. NEW OBSERVATIONS FOR AND XVI AND XVII

Observations of And XVI and XVII were made between 1-2 October, 2013, using the DEep Imaging Multi-Object Spectrograph (DEIMOS) on the Keck II telescope. DEIMOS is a slit-based spectrograph, and separate masks were designed for both objects that targeted stars on the red giant branches (RGBs) of the dSphs. To achieve spectra of the required S/N for determining velocities ($> 3 \text{ \AA}^{-1}$), only stars with apparent i -band magnitudes between $20.5 < i < 23.5$ were selected. The instrumental set-up for each mask used the 1200 line mm^{-1} grating (resolution of 1.4 \AA FWHM), and a central wavelength of 7800 \AA , giving spectral coverage from $\sim 5600 - 9800 \text{ \AA}$, isolating the region of the calcium triplet (Ca II) at $\lambda \sim 8500 \text{ \AA}$. The average seeing per mask was $0.8''$ and $1.0''$ respectively.

In this work, we combine our 2013 data for And XVII with an earlier mask, observed in September 2011 (Collins et al. 2013). The exposure time for the mask observed in 2011 was 3600s, while the two 2013 masks were observed for 7200s.

We reduce the resulting science spectra using a custom built pipeline, described in Ibata et al. (2011) and Collins et al. (2013). We derive velocities using the Ca II triplet absorption feature. Typically velocity uncertainties are $3-10 \text{ km s}^{-1}$. We correct these velocities to the heliocentric frame and for systematic shifts caused by misalignments of the slits. Additionally, for the And XVII data, we use velocities of 13 duplicate stars observed in both masks to check the measured offsets, resulting in more accurate velocity corrections.

2.1. Kinematics

For both And XVI and XVII, we aim to better constrain their systemic velocities, v_r , and velocity dispersions, σ_v , as they were previously measured from only a handful of stars (8 and 7 for And XVI and XVII respectively). First, we determine which observed stars are dSph members, and which are MW or M31 halo contaminants using a probabilistic method developed by Collins et al. (2013). We assign probability of a given star being a member of the dwarf galaxy using three criteria: (1) the position on the color magnitude diagram of the dwarf, (2) the distance from the center of the dwarf galaxy and (3) the velocity. The probability of membership is the product of these three criteria. For a detailed description of this method, see Collins et al. (2013).

In fig. 1, we display the results of this membership determination. The top two plots of fig. 1 summarise the kinematic properties of the And XVI and XVII fields. The top panels show a velocity histogram for all observed stars. Our technique hones in on cold velocity peaks located at $\sim -370 \text{ km s}^{-1}$ and $\sim -260 \text{ km s}^{-1}$ for And XVI and XVII respectively. The central panels show the distance from the center of the dSph as a function of radius. Here, the points are color-coded by their probability of membership. Open points represent stars for which the probability of membership is negligible. In the lower panel, we show the photometrically derived $[\text{Fe}/\text{H}]$ for each stars as a function of velocity, determined using Dartmouth isochrones (Dotter et al. 2008) with age 12 Gyr and $[\alpha/\text{Fe}] = +0.2$. In the lower two plots of fig. 1, we display the PAndAS CMDs (McConnachie et al. 2009) for both dSphs. These diagnostics isolate those stars belonging to And XVI and XVII, indicating 20 and 16 probable member stars ($P_{\text{member}} > 0.1$) respectively, more than doubling previous sample sizes. In the subsequent analysis, these probabilities act as weights for each star, allowing us to estimate all parameters for the satellites without having to make any subjective cuts on the data. In the case of And XVII, many of the stars have a low probability of membership ($P_{\text{member}} \lesssim 0.5$), as the systemic velocity of this object sits within 1σ of the M31 halo velocity ($v_{r,\text{halo}} = 300 \text{ km s}^{-1}$, $\sigma_{v,\text{halo}} \sim 90 \text{ km s}^{-1}$, e.g., Chapman et al. 2006; Kalirai et al. 2006), which is clearly visible as a non-negligible contaminant in the velocity histogram of And XVII. As such, the stars in And XVII also have non-negligible probabilities of being halo contaminants. As the weights are treated relative to those of the other stars in the mask, this does not have a huge impact on measurements of the systemic velocity and dispersion, aside from increasing the uncertainties in the measurements.

Using this information, we derive v_r and σ_v for each dSph using the grid-based maximum likelihood approach of Collins et al. (2013). We determine $v_r = -369.1^{+1.1}_{-1.3} \text{ km s}^{-1}$ and $\sigma_v = 5.8^{+1.1}_{-0.9} \text{ km s}^{-1}$ for And XVI, and $v_r = -264.3 \pm 2.5 \text{ km s}^{-1}$ and $\sigma_v = 6.5^{+3.3}_{-2.7} \text{ km s}^{-1}$ for And XVII. We find that the systemic velocity of And XVI is in good agreement with the Tollerud et al. (2012) value of $v_r = -367.3 \pm 2.8$. The velocity dispersion we measure here is consistent with the Tollerud et al. (2012) value of $\sigma_v = 3.8 \pm 2.9 \text{ km s}^{-1}$, but is nominally higher. For And XVII, we measure a significantly different v_r from the

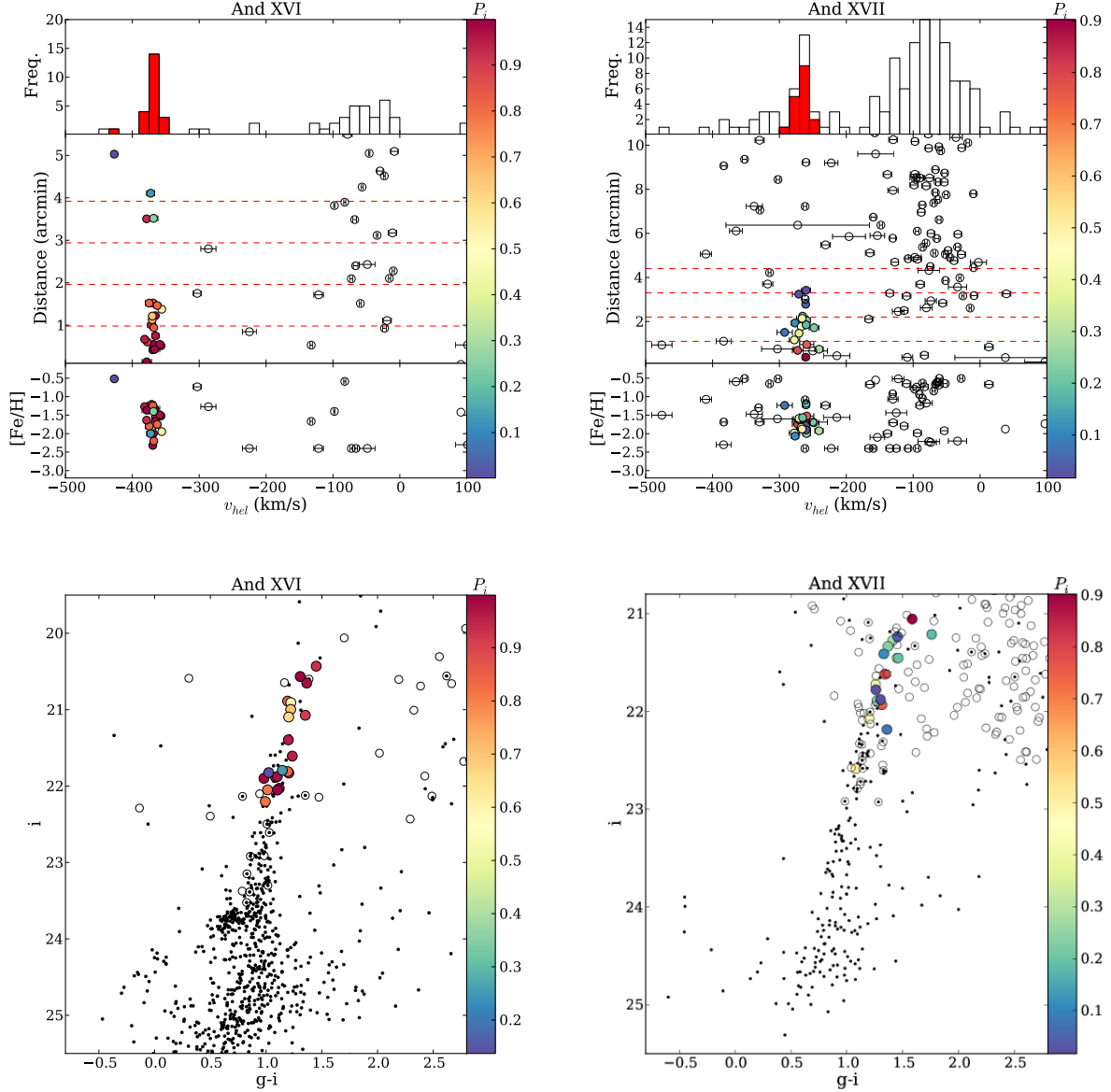


FIG. 1.— **Top:** Kinematics for And XVI (left) and XVII (right). The top panels show velocity histograms of all stars observed. Probable members are highlighted as the red histogram. The center panel shows the distance of each star from the center of the dSph as a function of velocity. Here, stars are colour coded by their probability of membership. Stars with a negligible probability of membership are shown as open circles. Dashed red lines represent $1, 2, 3$ and $4 \times r_{\text{half}}$ for the dSph. The lower panel shows the photometric metallicities for stars as a function of velocity. Again, stars are color-coded by probability of membership. **Bottom:** PAndAS CMDs for And XVI (left) and XVII (right) for all sources within $2 \times r_{\text{half}}$ of the dSph. Stars observed with DEIMOS are color-coded by membership probability.

Collins et al. (2013) value of $v_r = -251.6^{+1.8}_{-2.0} \text{ km s}^{-1}$ (almost 3σ discrepant). This is due to our improvement in calibrating systematics in our velocity measurements by using repeat observations of 13 stars that are common to both masks. When stars are miscentered within their milled slits, shifts in velocity of $10 - 15 \text{ km s}^{-1}$ can occur, and normally this is corrected for by measuring the telluric lines also imprinted onto a stars spectrum, and cross-correlating these telluric features with a rest-frame template. For faint stars (with low S/N) this technique can introduce more noise into velocity measurements (as demonstrated in Collins et al. 2010, 2013). With the higher S/N sources in our 2nd And XVII mask (which

had double the exposure time), we were better able to correct for misalignment in the second mask, then use the velocities for the 13 duplicates to refine our velocity measurements for the 2011 mask.

2.2. Metallicities

We determine the average metallicities of the systems from a co-addition of all member spectra with $S/N > 3 \text{ \AA}^{-1}$ in continuum. This leaves us with a sample of 12 stars in And XVI and 7 in And XVII. We perform a weighted co-addition of these spectra (using both S/N and P_{member}). To determine $[\text{Fe}/\text{H}]$, we fit the continuum and Ca II lines simultaneously as a poly-

nomial and triple Gaussian. We check that each line is uncontaminated by skylines, and then measure $[\text{Fe}/\text{H}]$ using the Starkenburg et al. (2010) relation, adapted to utilize all 3 lines of the triplet for And XVI and XVII (Collins et al. 2013). The resulting spectra are shown in fig. 2. We determine $[\text{Fe}/\text{H}] = -2.0 \pm 0.1$ for And XVI and $[\text{Fe}/\text{H}] = -1.7 \pm 0.1$ for And XVII. These values agree well with previous spectroscopic measurements of $[\text{Fe}/\text{H}] = -2.1 \pm 0.2$ and $[\text{Fe}/\text{H}] = -1.9 \pm 0.2$ (Letarte et al. 2009; Collins et al. 2013), and photometric estimates of $[\text{Fe}/\text{H}] = -1.7$ (Ibata et al. 2007) and $[\text{Fe}/\text{H}] = -1.9$ Irwin et al. (2008).

3. COMPARING DSPHS IN AND OUT OF THE SATELLITE PLANE

With secure kinematics for And XVI and XVII, we possess reliable measurements for 12 of the 14 dSphs in the M31 satellite plane. Two objects (And XI and XII) have barely resolved velocity dispersions, so we remove them from this analysis. Using this sample, we make a global comparison of dSphs on and off the M31 satellite plane, and search for evidence of radically different formative or evolutionary histories for these two populations.

In fig. 3 we compare the different parameter spaces probed by dynamic and photometric observations of LG dSphs. The luminosities and half-light radii for the dSphs are collated from Tolstoy et al. (2009); McConnachie (2012); Martin et al. (2013b,a), except for those M31 dSphs covered by the PAndAS survey (24 objects), where revised measurements from Martin et al. (in prep.) are employed. The differences between the Martin et al. measurements, and previously reported values, are within 1σ of one another. The dynamics are assembled from Walker et al. (2009); Koposov et al. (2011); Tollerud et al. (2012); Ho et al. (2012); Collins et al. (2013); Tollerud et al. (2013); Kirby et al. (2013a); Martin et al. (2014) and, for And XXI, Collins et al. (in prep). Spectroscopic metallicities are also taken from these works, plus Ho et al. (2014) and Vargas et al. (2014).

The top-left panel of fig. 3 shows size vs. luminosity for LG dSph galaxies. The gray shaded region represents the best fit relation and 1σ scatter measured by Brasseur et al. (2011) to these properties for MW and M31 dwarf galaxies. And XVI and XVII agree well with this relation. To determine whether there is a significant difference between the on- and off-plane dwarfs, we perform a linear fit, where $\log(r_{\text{half}}) = A + B \log(M_V + 6)$ to 10,000 Monte Carlo resamples of the M31 data. The median results are plotted as the dashed and dot dashed lines in Fig. 3. Comparing the distributions of the slope/intercepts (shown in table 1), we find the on- and off-plane values agree at $< 1\sigma$, meaning that the two populations appear to be indistinguishable. We perform a similar analysis in luminosity-metallicity space (shown in the top-right panel of Fig. 3. Here, the gray band represents the universal mass-metallicity relation of Kirby et al. (2013b). We find that the linear fits to the resampled on- and off-plane data (where $[\text{Fe}/\text{H}] = A + B \log(L_V/10^6)$) are again in accord with one another at $< 1\sigma$ (see table 1). If the planar dSphs had formed out of the gas rich tidal tails of a merger 5-8 Gyrs ago, their initial chemical enrichment may have been markedly different to those outside the plane, resulting in a different $L - [\text{Fe}/\text{H}]$ relation (e.g., Weibacher

TABLE 1
BEST FIT RELATIONS FOR ON- AND OFF-PLANE
M31 dSPHS IN SIZE, LUMINOSITY, METALLICITY
AND MASS PARAMETER SPACES.

Parameter	On-plane	Off-plane
<i>L vs. r_{half}</i>		
Intercept, A (dex)	2.2 ± 0.2	2.2 ± 0.2
Slope, B (dex)	-0.09 ± 0.07	-0.14 ± 0.05
<i>L vs. $[\text{Fe}/\text{H}]$</i>		
Intercept, A (dex)	-1.7 ± 0.1	-1.8 ± 0.1
Slope, B (dex)	0.2 ± 0.2	0.3 ± 0.2
<i>r_{half} vs. σ_v</i>		
V_{max} (km s^{-1})	12.9 ± 1.0	13.0 ± 1.2
R_S (pc)	442 ± 168	295 ± 124

et al. 2003). And yet there is no evidence for this in the data.

Finally, the lower 2 panels of fig. 3 inform us about the masses and dark matter content of the MW and M31 dSphs. The left panel shows the relationship between the size and the velocity dispersions (an indicator of mass) of LG dSphs. The shaded region shows the range of NFW halo profiles that best represent the masses of MW and M31 dSphs (Collins et al. 2014). And XVI and XVII now agree very well with these relations, whereas previously they were tentatively low mass outliers (Tollerud et al. 2012; Collins et al. 2013). We fit NFW profiles (Navarro et al. 1997, with the maximum circular velocity (V_{max}) and scale radius (R_S) of the halo as free parameters) to our resampled on- and off-plane data. Once again, the on-plane and off-plane fits agree at $< 1\sigma$ (see table 1), suggesting no significant differences between these two populations. This is further reflected in the lower right panel of fig. 3 where we present mass (calculated from the velocity dispersion using the Walker et al. 2009 mass estimator) vs. luminosity within the half-light radius for LG dSphs. Objects that possess no significant dark matter component (as in tidally formed dwarf galaxies) are expected to reside within the green shaded region. All the dSphs in this study are consistent with having $[M/L]_{\text{half}} \gtrsim 10 M_{\odot}/L_{\odot}$, implying that they are dark matter dominated systems, with no apparent difference between the dSphs in the plane vs. those outside of the plane.

Another argument against a tidal formation scenario for the planar satellites is the ages of the stars in these systems. Photometry of these systems suggest that they are ‘old’, and possess many stars with ages > 2 Gyr (Martin et al. 2006, 2009; McConnachie 2012), and often possess RR-lyrae stars, which are at least 10 Gyrs old (e.g., And II, Pritzl et al. 2004). Recently Weisz et al. (2014) measured and compared the SFHs of And II (an off-plane satellite) and And XVI (on-plane) using HST imaging. They found that both had similar, extended star formation histories, with 50 – 70% of their stars forming 12 to 5 Gyrs ago. They were also both quenched 5 Gyrs ago, right around the time of the merger purported to have created the plane by Hammer et al. (2013). Thus, if the plane of satellites formed tidally, the merger that created them would need to have occurred at very early times (~ 10 Gyrs ago). As this is based on only 2 objects, a complete survey of the SFHs of M31 dSphs is necessary to validate this.

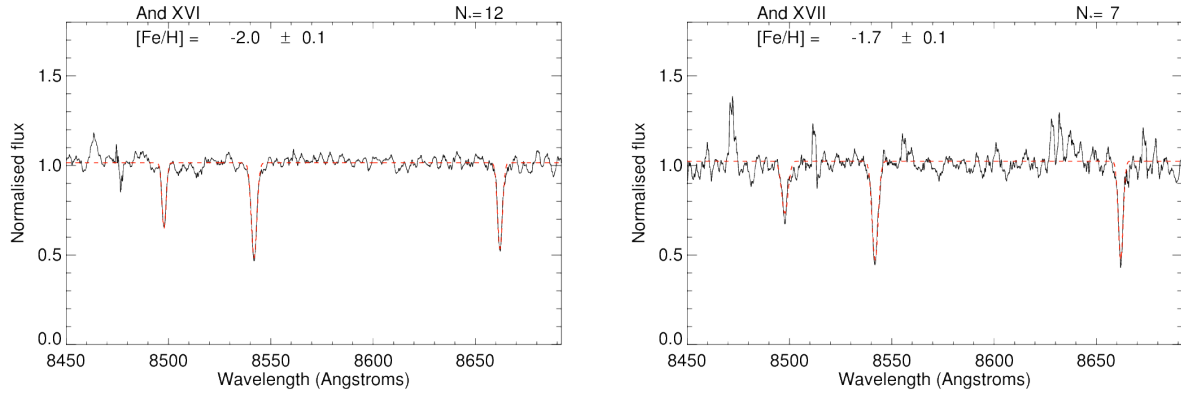


FIG. 2.— Co-added spectra for And XVI (left) and XVII (right), constructed for all probable member stars with $S/N > 3 \text{ \AA}^{-1}$.

Given that, for every observation we can make in these systems, there are no measurable differences between on- and off-plane dSphs, it is unlikely that the two populations formed in a radically different fashion. Their spatial orientations are all that separates them. As such, any attempt to model the formation of this unusually thin plane must also explain the commonalities between the on-plane and off-plane galaxies.

4. CONCLUSIONS

In order to create a more uniform sample for analysis of the in-plane M31 dSphs, we have presented robust kinematic properties for the M31 dSphs, And XVI and XVII. From samples of 20 and 16 member stars respectively, we derive $v_r = -369.1^{+1.1}_{-1.3} \text{ km s}^{-1}$ and $\sigma_v = 5.8^{+1.1}_{-0.9} \text{ km s}^{-1}$ for And XVI and $v_r = -264.3 \pm 2.5 \text{ km s}^{-1}$ and $\sigma_v = 6.5^{+3.3}_{-2.7} \text{ km s}^{-1}$ for And XVII. We measure average spectroscopic metallicities for both dSphs, finding $[\text{Fe}/\text{H}] = -2.0 \pm 0.1$ for And XVI and $[\text{Fe}/\text{H}] = -1.7 \pm 0.1$ for And XVII. When comparing their properties to those of other LG dSphs, we find they are consistent with established trends between size, luminosity, chemistry, and mass.

We also compare the structural and kinematic properties of 12 on-plane M31 dSphs with 18 off-plane dSphs to assess whether these two populations differ in any way. We find that the only observation that separates them is their spatial alignment. When comparing their sizes, luminosities, masses, metallicities and star formation histories, these populations are indistinguishable from one

another. This argues against any radically different formation mechanism for the on-plane dSphs, such as the formation of these objects in a gas rich merger 5-8 Gyrs (Hammer et al. 2013). Any future efforts to understand the formation of such an unusually thin plane of satellites must therefore also account for these universal trends.

ACKNOWLEDGMENTS

M.L.M.C. acknowledges funding from the European Research Council under the EUs FP 7 ERC Grant Agreement n. [321035]. Support for this work was provided by NASA through Hubble Fellowship grant #51337 awarded by the Space Telescope Science Institute, which is operated by the Association of Universities for Research in Astronomy, Inc., for NASA, under contract NAS 5-26555.

R.I. gratefully acknowledges support from the Agence Nationale de la Recherche through grant POMMME (ANR 09-BLAN-0228).

N.F.M acknowledges the CNRS for support through PICS project PICS06183.

G.F.L. acknowledges financial support through an ARC Future Fellowship (FT100100268) and ARC Discovery Project (DP110100678).

The data presented herein were obtained at W.M. Keck Observatory, which is operated as a scientific partnership among the California Institute of Technology, the University of California and the National Aeronautics and Space Administration. The Observatory was made possible by the generous financial support of the W.M. Keck Foundation.

REFERENCES

- Bellazzini, M., Oosterloo, T., Fraternali, F., & Beccari, G. 2013, *A&A*, 559, L11
- Brasseur, C. M., Martin, N. F., Macciò, A. V., Rix, H.-W., & Kang, X. 2011, *ApJ*, 743, 179
- Chapman, S. C., Ibata, R., Lewis, G. F., Ferguson, A. M. N., Irwin, M., McConnachie, A., & Tanvir, N. 2006, *ApJ*, 653, 255
- Collins, M. L. M., Chapman, S. C., Irwin, M. J., Martin, N. F., Ibata, R. A., Zucker, D. B., Blain, A., Ferguson, A. M. N., Lewis, G. F., McConnachie, A. W., & Peñarrubia, J. 2010, *MNRAS*, 407, 2411
- Collins, M. L. M., Chapman, S. C., Rich, R. M., Ibata, R. A., Martin, N. F., Irwin, M. J., Bate, N. F., Lewis, G. F., Peñarrubia, J., Arimoto, N., Casey, C. M., Ferguson, A. M. N., Koch, A., McConnachie, A. W., & Tanvir, N. 2013, *ApJ*, 768, 172
- . 2014, *ApJ*, 783, 7
- Conn, A. R., Lewis, G. F., Ibata, R. A., Parker, Q. A., Zucker, D. B., McConnachie, A. W., Martin, N. F., Valls-Gabaud, D., Tanvir, N., Irwin, M. J., Ferguson, A. M. N., & Chapman, S. C. 2013, *ApJ*, 766, 120
- Dotter, A., Chaboyer, B., Jevremović, D., Kostov, V., Baron, E., & Ferguson, J. W. 2008, *ApJS*, 178, 89
- Hammer, F., Yang, Y., Fouquet, S., Pawlowski, M. S., Kroupa, P., Puech, M., Flores, H., & Wang, J. 2013, *MNRAS*, 431, 3543
- Hammer, F., Yang, Y. B., Wang, J. L., Puech, M., Flores, H., & Fouquet, S. 2010, *ApJ*, 725, 542
- Ho, N., Geha, M., Munoz, R. R., Guhathakurta, P., Kalirai, J., Gilbert, K. M., Tollerud, E., Bullock, J., Beaton, R. L., & Majewski, S. R. 2012, *ApJ*, 758, 124

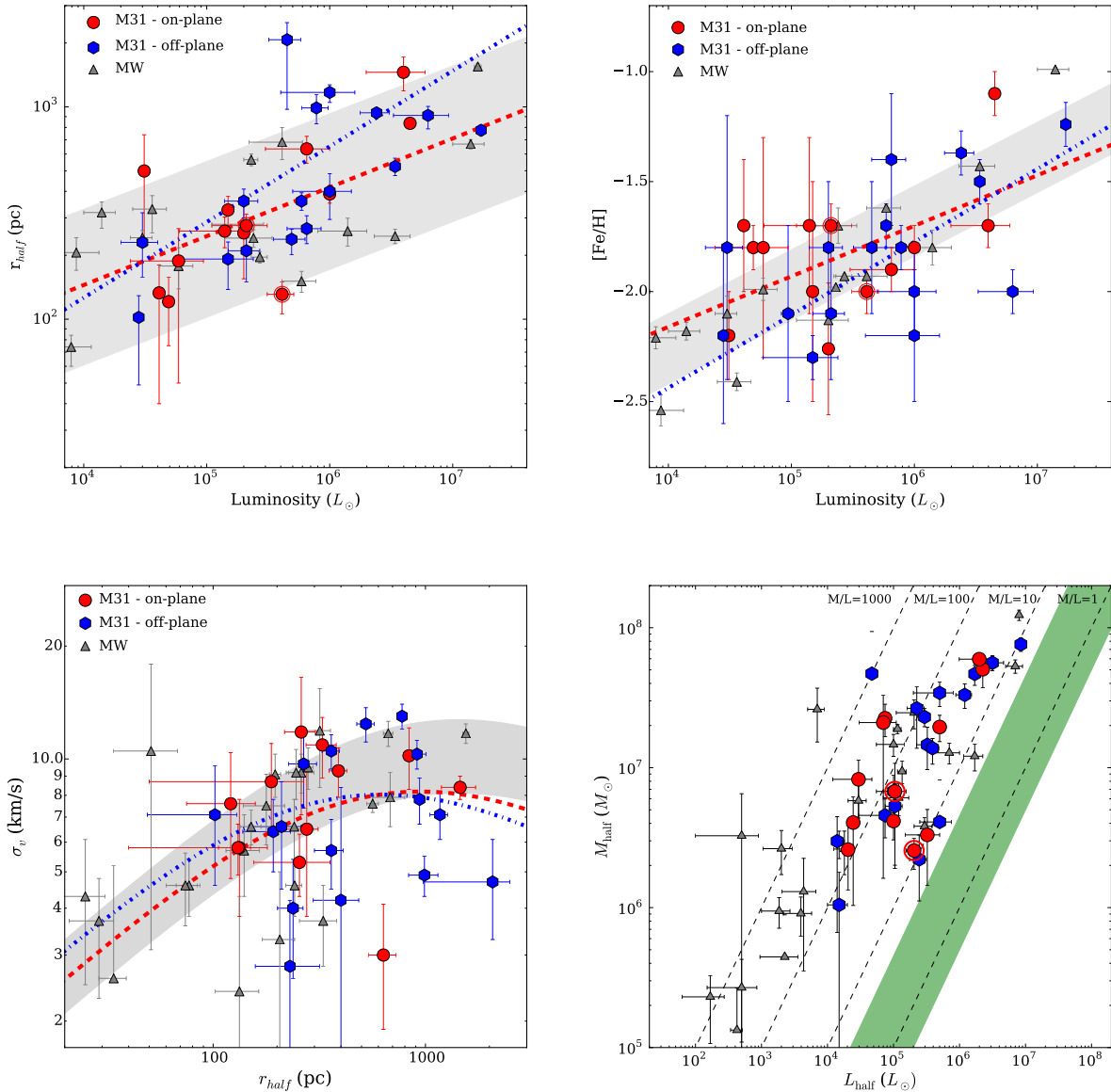


FIG. 3.— A comparison of the properties of on- and off-plane M31 satellites (shown as red circles and blue hexagons respectively) with MW dSphs (gray triangles), and various dSph relations. And XVI and XVII are shown as encircled red points. In all cases there are no significant differences between M31 on-plane and off-plane dSphs. **Top left:** L vs. r_{half} for LG dSphs. The Brasseur et al. (2011) relation for LG dSphs is shown as the gray band. **Top right:** L vs. $[\text{Fe}/\text{H}]$ for LG dSphs. The gray band represents the Kirby et al. (2013b) mass-metallicity relation. **Bottom left:** r_{half} vs. σ_v for LG dSphs. Here, the gray band represents the range of NFW halo mass profiles that best encapulate the dSphs of the MW and M31. **Bottom right:** L_{half} vs. M_{half} for LG dSphs. The dashed lines represent constant mass-to-light ratios of 1, 10, 100 and 1000 from right to left. The shaded green region indicates the parameter space occupied by objects with no significant dark matter component. All the LG dSphs fall above this limit, and are likely dark matter dominated.

Ho, N., Geha, M., Tollerud, E., Zinn, R., Guhathakurta, P., & Vargas, L. 2014, ArXiv e-prints
 Ibata, N. G., Ibata, R. A., Famaey, B., & Lewis, G. F. 2014a, Nature, 511, 563
 Ibata, R., Martin, N. F., Irwin, M., Chapman, S., Ferguson, A. M. N., Lewis, G. F., & McConnachie, A. W. 2007, ApJ, 671, 1591
 Ibata, R., Sollima, A., Nipoti, C., Bellazzini, M., Chapman, S. C., & Dalessandro, E. 2011, ApJ, 738, 186
 Ibata, R. A., Ibata, N. G., Lewis, G. F., Martin, N. F., Conn, A., Elahi, P., Arias, V., & Fernando, N. 2014b, ApJ, 784, L6

Ibata, R. A., Lewis, G. F., Conn, A. R., Irwin, M. J., McConnachie, A. W., Chapman, S. C., Collins, M. L., Fardal, M., Ferguson, A. M. N., Ibata, N. G., Mackey, A. D., Martin, N. F., Navarro, J., Rich, R. M., Valls-Gabaud, D., & Widrow, L. M. 2013, Nature, 493, 62
 Irwin, M. J., Ferguson, A. M. N., Huxor, A. P., Tanvir, N. R., Ibata, R. A., & Lewis, G. F. 2008, ApJ, 676, L17
 Kalirai, J. S., Gilbert, K. M., Guhathakurta, P., Majewski, S. R., Ostheimer, J. C., Rich, R. M., Cooper, M. C., Reitzel, D. B., & Patterson, R. J. 2006, ApJ, 648, 389
 Kirby, E. N., Boylan-Kolchin, M., Cohen, J. G., Geha, M., Bullock, J. S., & Kaplinghat, M. 2013a, ApJ, 770, 16
 Kirby, E. N., Cohen, J. G., Guhathakurta, P., Cheng, L., Bullock, J. S., & Gallazzi, A. 2013b, ApJ, 779, 102

- Kirby, E. N., Lanfranchi, G. A., Simon, J. D., Cohen, J. G., & Guhathakurta, P. 2011, *ApJ*, 727, 78
- Koposov, S. E., Gilmore, G., Walker, M. G., Belokurov, V., Wyn Evans, N., Fellhauer, M., Gieren, W., Geisler, D., Monaco, L., Norris, J. E., Okamoto, S., Penarrubia, J., Wilkinson, M., Wyse, R. F. G., & Zucker, D. B. 2011, *ArXiv e-prints*, 1105.4102
- Letarte, B., Chapman, S. C., Collins, M., Ibata, R. A., Irwin, M. J., Ferguson, A. M. N., Lewis, G. F., Martin, N., McConnachie, A., & Tanvir, N. 2009, *MNRAS*, 400, 1472
- Lynden-Bell, D. 1976, *MNRAS*, 174, 695
- Martin, N. F., Ibata, R. A., Irwin, M. J., Chapman, S., Lewis, G. F., Ferguson, A. M. N., Tanvir, N., & McConnachie, A. W. 2006, *MNRAS*, 371, 1983
- Martin, N. F., McConnachie, A. W., Irwin, M., Widrow, L. M., Ferguson, A. M. N., Ibata, R. A., Dubinski, J., Babul, A., Chapman, S., Fardal, M., Lewis, G. F., Navarro, J., & Rich, R. M. 2009, *ApJ*, 705, 758
- Martin, N. F., Schlafly, E. F., Slater, C. T., Bernard, E. J., Rix, H.-W., Bell, E. F., Ferguson, A. M. N., Finkbeiner, D. P., Laevens, B. P. M., Burgett, W. S., Chambers, K. C., Draper, P. W., Hodapp, K. W., Kaiser, N., Kudritzki, R.-P., Magnier, E. A., Metcalfe, N., Morgan, J. S., Price, P. A., Tonry, J. L., Wainscoat, R. J., & Waters, C. 2013a, *ApJ*, 779, L10
- Martin, N. F., Slater, C. T., Schlafly, E. F., Morganson, E., Rix, H.-W., Bell, E. F., Laevens, B. P. M., Bernard, E. J., Ferguson, A. M. N., Finkbeiner, D. P., Burgett, W. S., Chambers, K. C., Hodapp, K. W., Kaiser, N., Kudritzki, R.-P., Magnier, E. A., Morgan, J. S., Price, P. A., Tonry, J. L., & Wainscoat, R. J. 2013b, *ApJ*, 772, 15
- Martin, N. F., Chambers, K. C., Collins, M. L., Ibata, R. A., Rich, R. M., Bell, E. F., Bernard, E. J., Ferguson, A. M. N., Flewelling, H., Kaiser, N., Magnier, E. A., Tonry, J. L., Wainscoat, R. J., *ApJ*, 793, 14
- McConnachie, A. W. 2012, *AJ*, 144, 4
- McConnachie, A. W. et al. 2009, *Nature*, 461, 66
- Navarro, J. F., Frenk, C. S., & White, S. D. M. 1997, *ApJ*, 490, 493
- Pawlowski, M. S., Famaey, B., Jerjen, H., Merritt, D., Kroupa, P., Dabringhausen, J., Lüghausen, F., Forbes, D. A., Hensler, G., Hammer, F., Puech, M., Fouquet, S., Flores, H., & Yang, Y. 2014, *MNRAS*, 442, 2362
- Pawlowski, M. S., Kroupa, P., & Jerjen, H. 2013, *MNRAS*, 435, 1928
- Pawlowski, M. S., Pflamm-Altenburg, J., & Kroupa, P. 2012, *MNRAS*, 423, 1109
- Pritzl, B. J., Armandroff, T. E., Jacoby, G. H., & Da Costa, G. S. 2004, *AJ*, 127, 318
- Starkenburger, E., Hill, V., Tolstoy, E., González Hernández, J. I., Irwin, M., Helmi, A., Battaglia, G., Jablonka, P., Tafelmeyer, M., Shetrone, M., Venn, K., & de Boer, T. 2010, *A&A*, 513, A34+
- Tollerud, E. J., Beaton, R. L., Geha, M. C., Bullock, J. S., Guhathakurta, P., Kalirai, J. S., Majewski, S. R., Kirby, E. N., Gilbert, K. M., Yniguez, B., Patterson, R. J., Ostheimer, J. C., Cooke, J., Dorman, C. E., Choudhury, A., & Cooper, M. C. 2012, *ApJ*, 752, 45
- Tollerud, E. J., Geha, M. C., Vargas, L. C., & Bullock, J. S. 2013, *ArXiv e-prints*
- Tolstoy, E., Hill, V., & Tosi, M. 2009, *ARA&A*, 47, 371
- Vargas, L. C., Geha, M. C., & Tollerud, E. J. 2014, *ApJ*, 790, 73
- Walker, M. G., Mateo, M., Olszewski, E. W., Peñarrubia, J., Wyn Evans, N., & Gilmore, G. 2009, *ApJ*, 704, 1274
- Walker, M. G., McGaugh, S. S., Mateo, M., Olszewski, E. W., & Kuzio de Naray, R. 2010, *ApJ*, 717, L87
- Weilbacher, P. M., Duc, P.-A., & Fritze-v. Alvensleben, U. 2003, *A&A*, 397, 545
- Weisz, D. R., Skillman, E. D., Hidalgo, S. L., Monelli, M., Dolphin, A. E., McConnachie, A., Bernard, E. J., Gallart, C., Aparicio, A., Boylan-Kolchin, M., Cassisi, S., Cole, A. A., Ferguson, H. C., Irwin, M., Martin, N. F., Mayer, L., McQuinn, K. B. W., Navarro, J. F., & Stetson, P. B. 2014, *ApJ*, 789, 24